Available online at www.sciencedirect.com

SciVerse ScienceDirect

Ceramics International 39 (2013) 2535–2543

CERAMICS INTERNATIONAL

www.elsevier.com/locate/ceramint

Microstructure and electrical properties of zirconia and composite nanostructured ceramics sintered by different methods

Bogdan Stefan Vasile[a], Ecaterina Andronescu[a], Cristina Ghitulica[a,*], Otilia Ruxandra Vasile[a], Lavinia Curechiu[b], Rares Scurtu[c], Eugeniu Vasile[d], Roxana Trusca[d], Livia Pall[a], Virgil Aldica[e]

[a]*University POLITEHNICA of Bucharest, Faculty of Applied Chemistry and Material Science, Department of Oxide Materials and Nanomaterials, No. 1-7 Gh. Polizu Street, 011061 Bucharest, Romania*

[b]*Department of Physics, Alexandru Ioan Cuza University, Bulevardul Carol I, 11, 700506 Iasi, Romania*

[c]*Romanian Academy, Institute of Physical Chemistry, No. 202 Splaiul Independentei Street, 060021 Bucharest, Romania*

[d]*Metav C.D., No. 31 C.A. Roseti Street, 020015 Bucharest, Romania*

[e]*National Institute for Materials Physics, Atomistilor 105, Magurele, Bucharest, Romania*

Received 23 August 2012; received in revised form 3 September 2012; accepted 4 September 2012
Available online 25 September 2012

Abstract

The aim of this study is the preparation and characterization of dense cubic zirconia ceramics and zirconia nanocomposites (reinforced with 5 wt% alumina). The powders were obtained through sol–gel methods and densified using classical sintering and spark plasma sintering (SPS) methods. The obtained ceramics were characterized through X-ray diffraction, scanning electron microscopy and impedance spectroscopy at room and high temperature. The average grain size of cubic zirconia particles was found to be approximately 8 and 2.5 μm for the classical sintering and 99 nm for SPS. The alumina particles in composites have an average grain size of 0.7 μm for classical sintering and 53 nm for SPS ones. The total conductivity for nanocomposites sintered through both methods was also determined.

Keywords: A. Sintering; B. Nanocomposites; C. Electrical properties; YSZ

1. Introduction

Yttria stabilized zirconia with cubic structure is by far the most widely used material for solid electrolytes, and applications could also be found in the ceramic insulators field. The use of these materials is of interest due to their high chemical stability in oxidizing and reducing atmosphere and high conductivity. The solid electrolyte is one of the main components of a combustion cell for high and medium operating temperatures, and the production of high performance materials for the solid electrolytes has been the key factor for an increased efficiency of energy conversion [1].

In stabilized zirconia, part of the Zr^{4+} atoms are replaced by Y^{3+} atoms, with the purpose of stabilizing the high temperature polymorphic modifications of zirconia, thus avoiding the volume variations caused by phase transformations. Moreover, this leads to the creation of oxygen vacancies, which are critical for the electrolyte properties.

The ionic conductivity is directly proportional to the quantity of O^{2-} anions that migrate. The maximum ionic conductivity in the zirconia based systems is observed when the concentration of acceptor type dopant is minimal, with the condition that zirconia is fully stabilized to the fluorine type cubic structure. Although there are many studies concerning electrical performance of yttria stabilized zirconia, most investigations were made on micrometer structured ceramics [2–6]. Consequently, the investigation on nanometric size ceramics and their

*Corresponding author. Tel./fax: +40 21 310 76 33.
E-mail address: cghitulica@yahoo.com (C. Ghitulica).

0272-8842/$ - see front matter © 2012 Elsevier Ltd and Techna Group S.r.l. All rights reserved.
http://dx.doi.org/10.1016/j.ceramint.2012.09.013

composites is necessary, in order to determine what changes in properties occur with the decrease of grain size from micrometers to nanometers.

Composite ceramic materials, with alumina, were prepared, in order to further enhance the mechanical properties of zirconia. In this case, alumina also acts as a sintering aid. Moreover, the electrical conductivity is improved and a lower thermal expansion coefficient is obtained. Also alumina has the effect of lowering the electrical conductivity at grain boundary and an increase in bulk conductivity is observed [7–10].

In the present work, the effect of alumina addition to yttria stabilized zirconia, with respect to electrical properties and microstructure of ceramic samples, for different sintering methods—spark plasma and classical sintering, was studied.

2. Experimental procedure

Cubic stabilized zirconia based ceramics and composites, reinforced with 5 wt% alumina were synthesized and characterized. The amount of yttrium oxide added to the zirconia is of 10 mol%. The zirconia nanopowder was synthesized through a simple sol–gel method, described in previous work. The average particle size of yttria stabilized zirconia nanopowder used is 14 nm [11].

The composite nanopowder was obtained by an unconventional method, schematically presented in Fig. 1, as follows: cubic yttria stabilized zirconia nanopowder, calcinated at 700 °C/2 h, was added to a mixture of alumina nitrate, citric acid and ethylene glycol, in water. The mixture was left on a magnetic stirrer for 120 min at 80 °C, in order to remove water. Gelification also occurred. After that, the gel was heat treated at 700 °C for 120 min, in order to remove all organic residues.

This type of procedure was followed in order to assure a better homogeneity of phases. This is proved through EDX elemental mapping, the results being shown in Fig. 2, for the ceramic powder thermally treated at 700 °C.

By analyzing the elemental mapping on the composite powder it can be observed that the distribution of all elements is highly homogeneous.

The ceramic materials were sintered by classical sintering and "spark plasma sintering" (SPS). In the first case, the powders were shaped by uniaxial pressing, followed by sintering in air, at 1600 °C for 120 min. The SPS obtained samples were first uniaxially pressed into a 30 mm graphite dye, by applying 15 MPa of pressure. After that the graphite dye was placed into the SPS equipment. The sintering temperature used was 1200 °C, with a heating rate of approximately 55 °C/min and the time at the highest temperature was 5 min. The sintering procedure used 110 MPa pressure and inert gas (Ar) atmosphere [12–15].

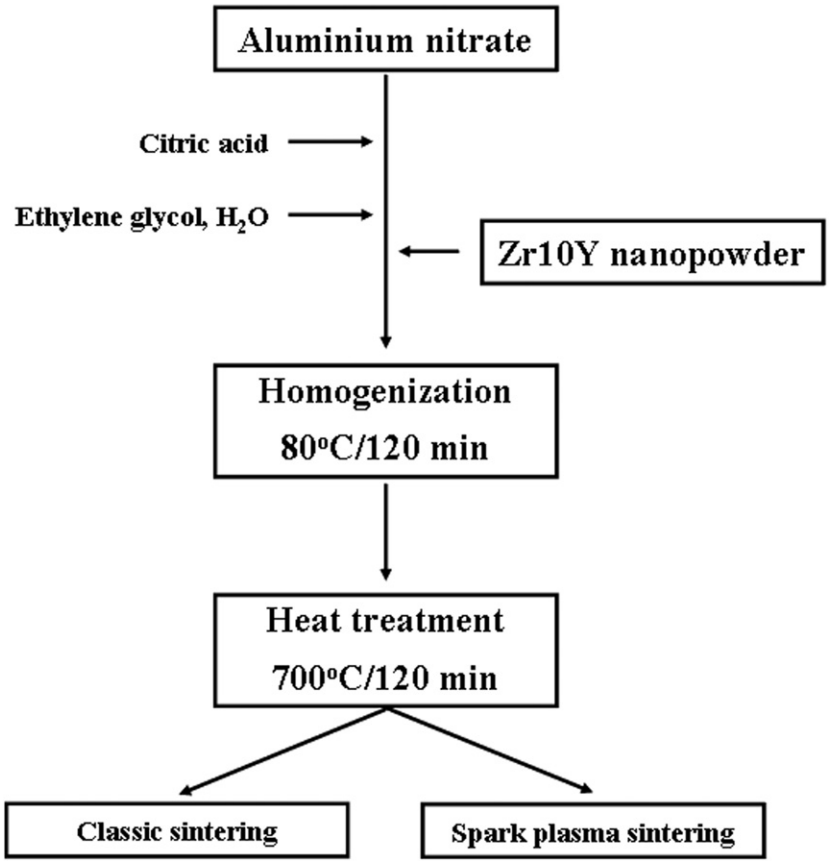

Fig. 1. Technological flow of composite powder preparation.

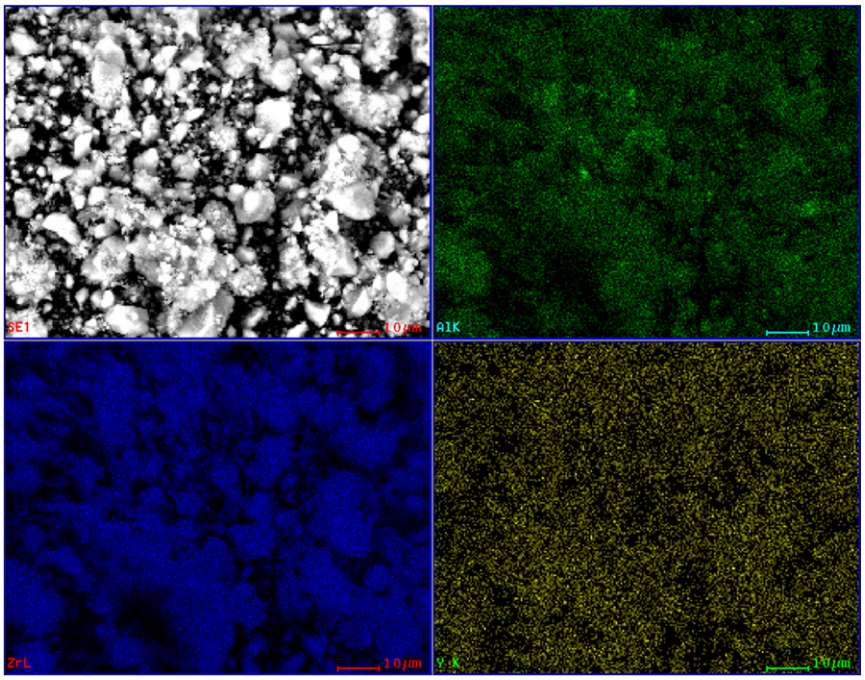

Fig. 2. SEM image coupled with EDX mapping showing the distribution of Al^{3+} (green), Y^{3+} (yellow) and Zr^{4+} (blue) in composite powder. (For interpretation of the references to color in this figure legend, the reader is referred to the web version of this article.)

The obtained samples were characterized by X-ray diffraction analysis using a Panalytical X'Pert Pro MPD equipment, with a CuKα radiation Ni filtered, over a scan range of $2\theta = 20^\circ$ to angle $2\theta = 80^\circ$.

Microstructural analysis was carried out using a Quanta inspect F scanning electron microscope (from FEI the Netherlands), with a resolution of 1.2 nm, equipped with an EDX detector at a resolution of 1.33 eV at MnKα.

Impedance spectroscopy investigation at room temperature was performed in a frequency range of 1 Hz–10 MHz using a Solartron impedance spectrometer and the impedance spectroscopic measurements at high temperature were conducted in air, in the temperature range of 550–1100 K and over the frequency range of 50 Hz–1 MHz, and amplitude of 100 mV with a Solartron 1260 FRA. The sample was placed in a ProboStat A sample holder (NorECs AS) and heated up using an Elite TSV12/50/300 vertical tube furnace. For all samples a gold coated contact was made in order to improve the connection between the ceramic sample and electrodes. IS data were corrected for the geometric factor of the sample (thickness/electrode area), the stray capacitance of the sample holder and the resistance and inductance of the measuring leads by using Zview fitting software.

3. Results and discussions

3.1. X-ray diffraction

The X-ray diffraction data, for both sintering methods and for the zirconia ceramics, as well as for the composite ceramics, are presented in Fig. 3.

The X-ray diffraction spectra obtained on yttria stabilized zirconia ceramics, sintered through SPS and classical sintering, and are showing a monophase composition—cubic solid solution of zirconia (ASTM 81-1551). The corresponding most intense diffraction peak is situated at an angle 2θ of 30.01°, characterized by (111) Miller indices.

In the case of composites, the spectra show cubic solid solution of zirconia as the majority component, and alpha alumina as the minority phase (ASTM 82-2081).

For the classically sintered composites alpha alumina diffraction peaks can be identified corresponding to the Miller indices (012), (113) and (116), while for the SPS samples only the peak for (012) Miller indices is present. Consequently, we may conclude that there is a preferential growth of crystals for the SPS samples. This is probably due to the fact that the sintering time and heating rate are very high.

3.2. Scanning electron microscopy

The electron micrographs obtained on cubic stabilized zirconia ceramics, through classical and spark plasma sintering, are presented in Fig. 4.

The classically sintered zirconia ceramic sample has a fine and dense microstructure, with grains of uniform shape, and polyhedral. The grains present a bimodal distribution, with an average grain size of 8 μm and 2.5 μm. It can be also observed that the bigger grains are formed by coalescence of smaller grains. The ceramic also presents well defined grain boundaries and in most of the cases triple junctions can be observed .

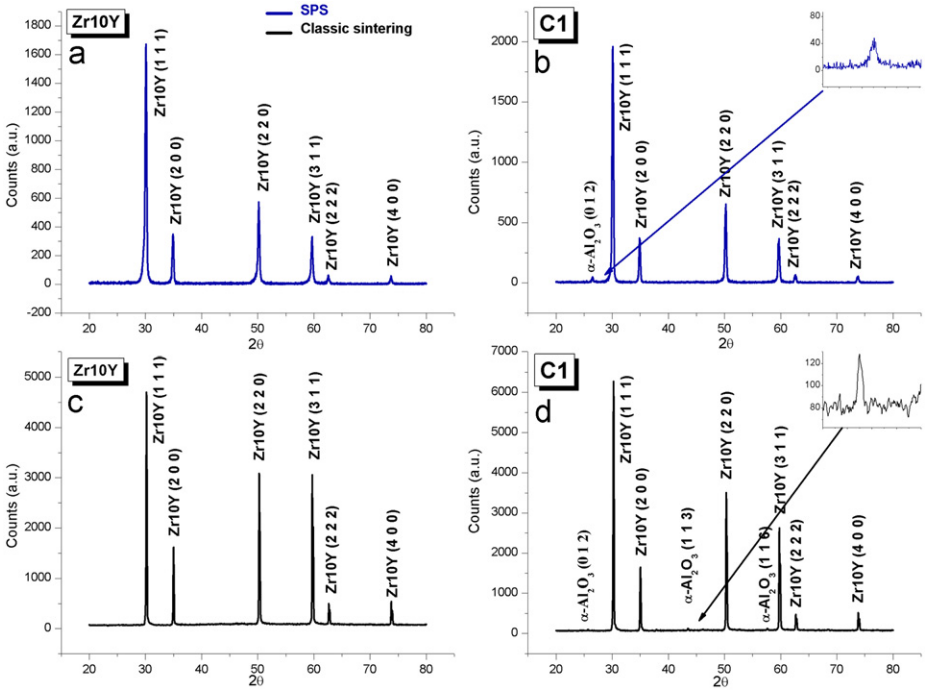

Fig. 3. X-ray diffraction spectra obtained on Zr10Y ceramic and composite C1 sintered through SPS (a) and (b); and classical sintering (c) and (d).

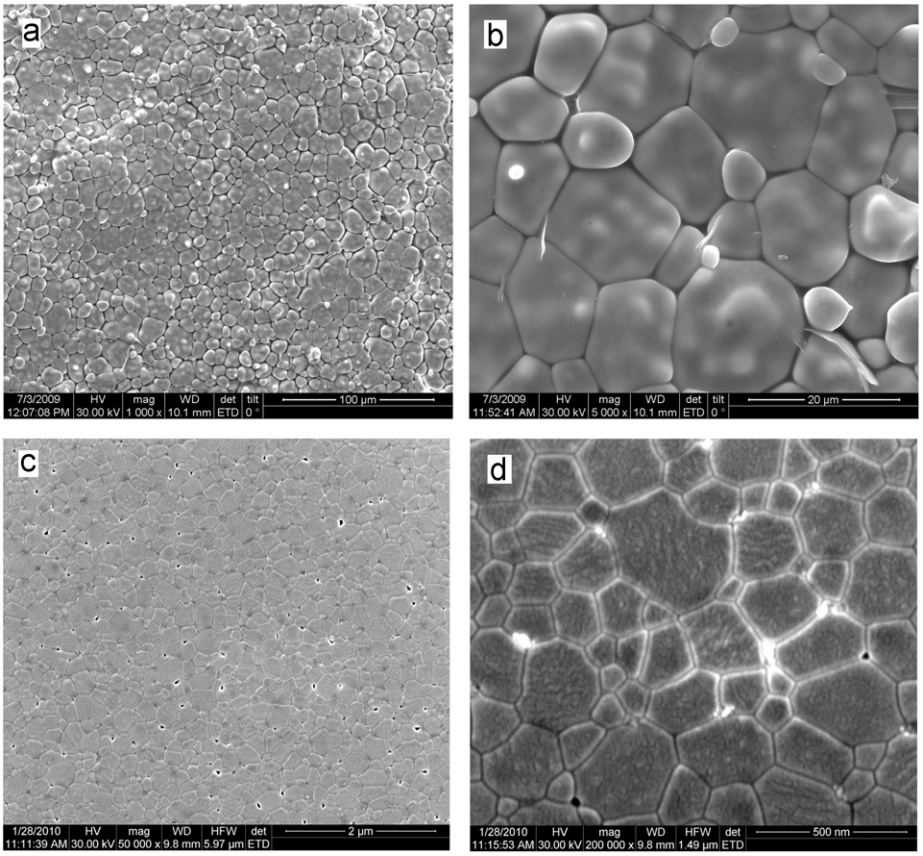

Fig. 4. SEM images of Zr10Y classically sintered (a), magnification of classically sintered Zr10Y (b), Zr10Y sintered through SPS (c) and of Zr10Y sintered through SPS (d).

In the case of yttria stabilized zirconia ceramics sintered through SPS, the SEM images indicate a denser microstructure and more homogeneous, compared with the classically sintered ceramic. In this case also, the distribution of grains is also bimodal, formed from polyhedral shaped grains, well faceted and with grain boundaries well

defined. This polyhedral shaped grain presents perfect triple junctions. The average grain size in this case is 99 nm.

The pores are present at the edge of grains, in much reduced quantity. The size of pores is about 20 nm.

The morphology of zirconia composites sintered through classical and spark plasma sintering is shown in the SEM images of Fig. 5. First of all the SEM images reveal the presence of two types of grains—large grains, attributed to stabilized zirconia, and smaller grains, attributed to alpha alumina.

The SEM images presented in Fig. 5(a), for the composite materials classically sintered, show a fine microstructure but not homogeneous, with intergranular pores not homogeneously distributed in the microstructure. The formation of conglomerates with various shapes can also be observed, around which can be noticed an agglomeration of porosity, forming tunnels in the microstructure.

The bigger grains, corresponding to the yttria stabilized zirconia, are not homogeneous in their shape and size, with dimensions as in the case of yttria stabilized zirconia grains.

The smaller grains, with an average size of 0.7 μm, are statistically distributed at the grain boundaries of stabilized zirconia. The connectivity degree for the composite material sintered by classical sintering is of 0–3 type, which is a Maxwell–Garnett type microstructure.

In the composite materials sintered through SPS, the highly homogenous character of the microstructure can be noticed. It is composed of 128 nm yttria stabilized zirconia grains, polyhedral, with perfect triple junctions and clearly evident grain boundaries. The alumina grains are uniformly distributed at the grain boundaries of zirconia grains, and have an average grain size of 53 nm, it can be seen from the backscatter images presented in Fig. 5(c) and (d). The alumina grains are isolated, so the nanocomposites, as in the case of classically sintered ones, present a Maxwell–Garnett type microstructure.

3.3. Electric properties

3.3.1. Impedance spectroscopy at room temperature

In the following, the dielectric properties of zirconia and composite ceramics are discussed, in correlation with the microstructure of samples.

The real and imaginary parts of dielectric permittivity for Zr10Y ceramics sintered through both methods are presented in Fig. 6(a) and (b). It can be observed that the permittivity for ceramics obtained by SPS is two orders of magnitude larger than in the case of the ceramics sintered by the classical method. This happens especially at low frequency, where the results are determined by extrinsic polarization mechanisms, like space charge or Maxwell–Wagner polarization. These

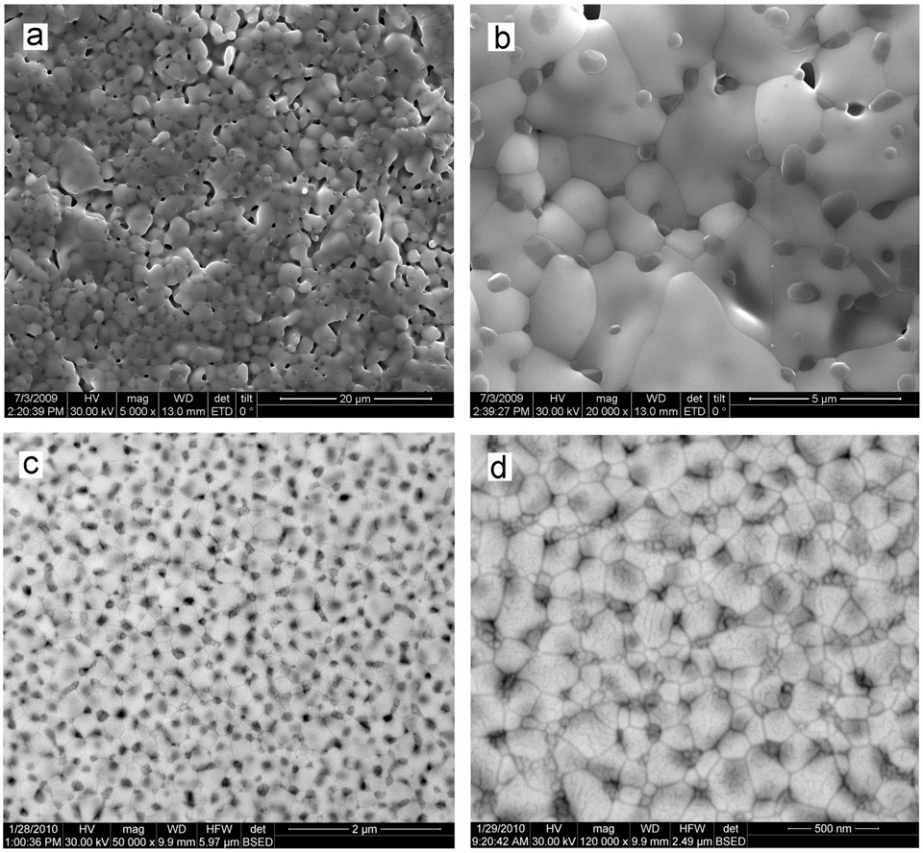

Fig. 5. SEM images of composite ceramic sintered through classical sintering (a), of composite ceramic sintered through classical sintering (b), composite ceramic sintered through SPS (c), and of composite ceramic sintered through SPS (d).

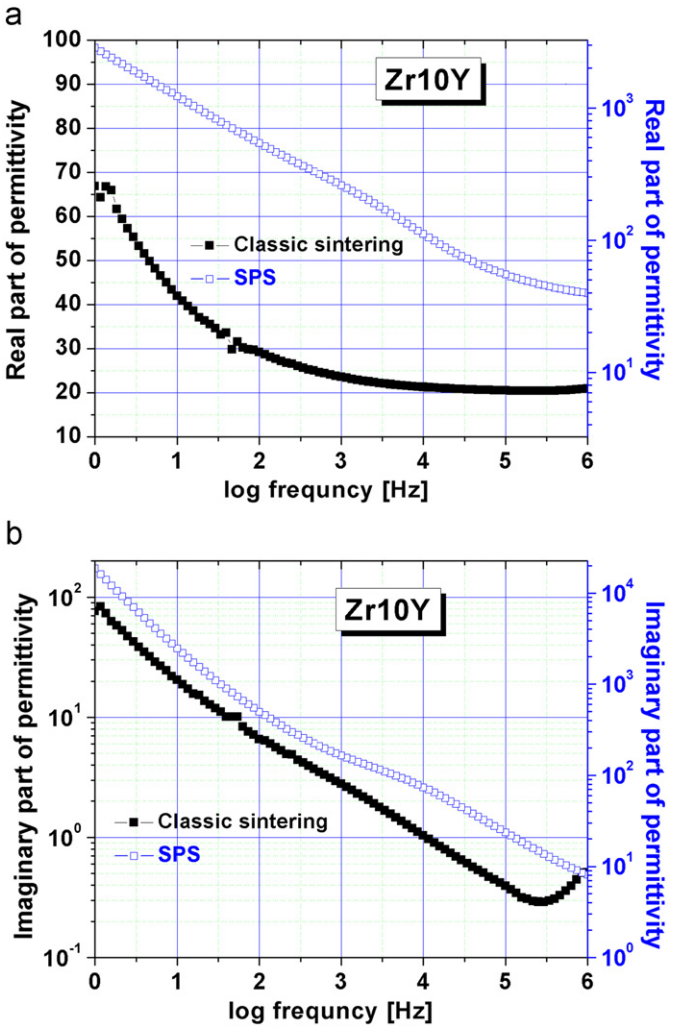

Fig. 6. Frequency dependence at room temperature for Zr10Y ceramics obtained by classical sintering and SPS: (a) real part of permittivity and (b) imaginary part of permittivity.

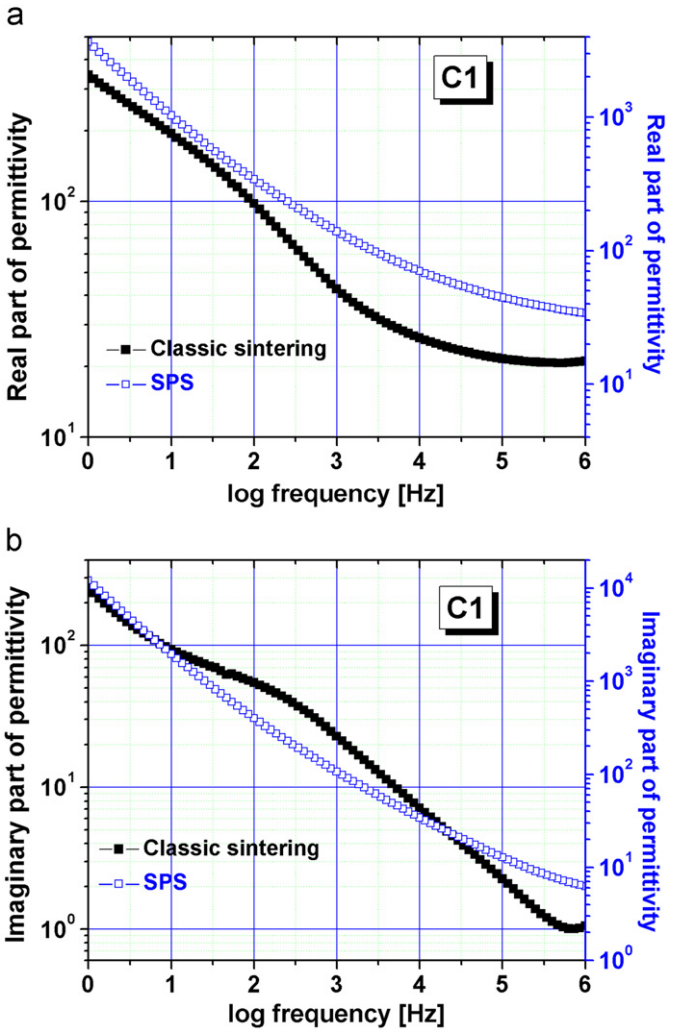

Fig. 7. Frequency dependence at room temperature for composite ceramics C1 obtained by classical sintering and SPS: (a) real part of permittivity and (b) imaginary part of permittivity.

values must be correlated with the imaginary part of permittivity and can be explained by the oxygen vacancies caused by the sintering method, SPS being a sintering method in reducing atmosphere. At high frequency (1 MHz), only the intrinsic properties of the material are influence the permittivity, and so the permittivity values are in the same order (20 for classical sintering and 39 for SPS ceramics).

The dielectric losses are larger than 1 in all frequency ranges for the SPS ceramics, while the others have lower values (< 0.5), for frequency above 100 Hz. In this case, it can be concluded that the ceramics sintered by the classic method are good dielectric materials for high frequency, at room temperature.

The dielectric properties of the composite ceramics sintered through SPS and the classical method are shown in Fig. 7(a) and (b). Also in this case, the ceramics sintered by SPS present a larger permittivity, due to interfacial polarization, that is generated by the oxygen vacancies. For the ceramics obtained by classical sintering, a Debye type relaxation was obtained with a relaxation time of 1.6×10^{-3} s.

The electrical modulus formalism is widely used to study electrical relaxation in electronically and ionically conducting materials, as it has the advantage of suppressing electrode polarization effects.

The complex dielectric modulus is defined as

$$M^*(f) = \frac{1}{\varepsilon^*}(f) = M'(f) + iM''(f), \quad (1)$$

With the real and imaginary parts given by

$$M'(f) = \frac{\varepsilon'(f)}{\varepsilon'^2}(f) + \varepsilon''^2(f), \; M''(f) = \frac{\varepsilon''(f)}{\varepsilon'^2}(f) + \varepsilon''^2(f) \quad (2)$$

The electric modulus corresponds to the relaxation of the electric field in the material when the electric displacement is maintained as constant [16,17]. The complex modulus $M^*(\omega)$ was firstly introduced to describe the dielectric response of non-conducting materials, but then it was applied also to materials with non-zero conductivity. The variation of its imaginary component as a function of frequency $M''(\omega)$ provides useful information concerning

the charge transport mechanism such as electrical transport and conductivity relaxation. The conductivity relaxation is indicated by the presence of a peak in the $M''(\omega)$ spectra and no peak would occur in the corresponding plot of $\varepsilon''(\omega)$, while the dielectric relaxation gives maxima, both in the imaginary part of permittivity $\varepsilon''(\omega)$ and of the dielectric modulus $M''(\omega)$ spectra. Comparisons of the complex ε^* and M^* representations have been used to distinguish localized dielectric relaxation processes from long-range conductivity [18,19].

The imaginary parts of dielectric modulus calculated for the present samples are shown in Fig. 8. In the investigated range of frequencies, the samples Zr10Y show one maximum of the imaginary part $M''(f)$ (Fig. 8(a)), while in $\varepsilon''(f)$ a monotonous decrease was obtained. In this case we have a relaxation given by conductivity. The effect of sintering condition was to move the maximum to a larger frequency.

In case of composite ceramics sintered by the classical method the peak position in $M''(f)$ (Fig. 8(b)) and $\varepsilon''(f)$ is the same, which implies a relaxation process. For the ceramic sintered by SPS only a maximum in M''(f) was obtained that also gives a conductivity relaxation.

In order to analyze the AC conductivity for the samples at room temperature the electrodynamics relation used was

$$\varepsilon''(f) = \frac{\sigma(f)}{2\pi f \varepsilon_0}, \tag{3}$$

which allowed computing the conductivity as a function of frequency from the relaxation of the imaginary part of permittivity. The comparative frequency-dependent conductivity results are shown in Fig. 9.

It can be observed that for the ceramics obtained by classical sintering at least two conducting mechanisms can be identified: one for frequency below 100 kHz and one for high frequencies. In case of the Zr10Y sample, by changing the sintering method a DC-conduction of 10^{-1} S/m^{-1} was obtained due to oxygen vacancies. In the composite ceramic sintered by SPS, only one conduction mechanism was obtained at room temperature.

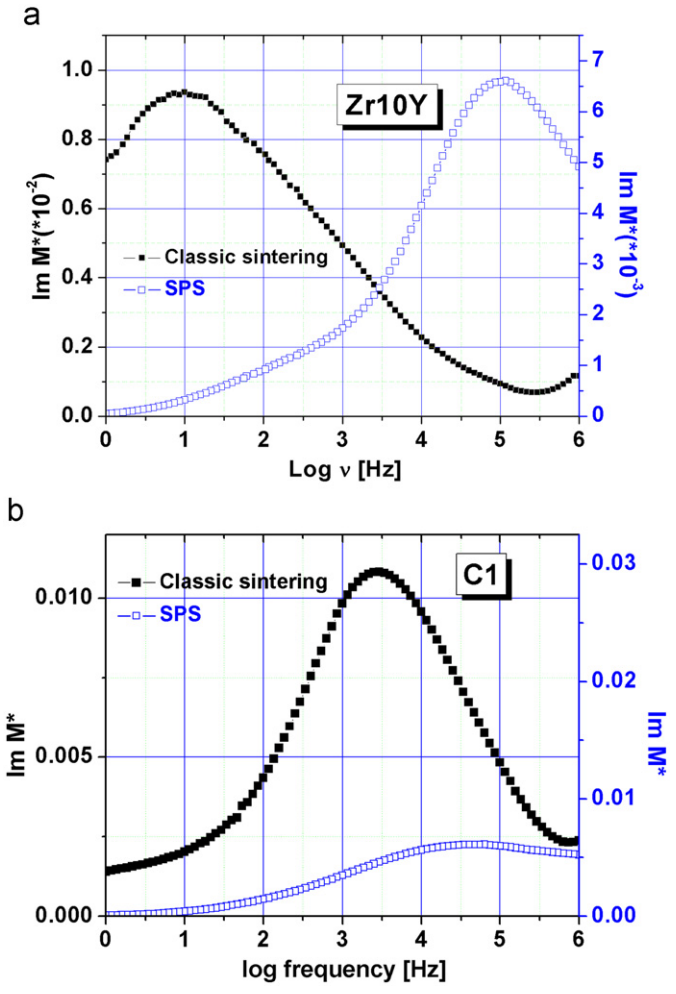

Fig. 8. Frequency dependence of imaginary part of dielectric modulus for (a) Zr10Y and (b) C1.

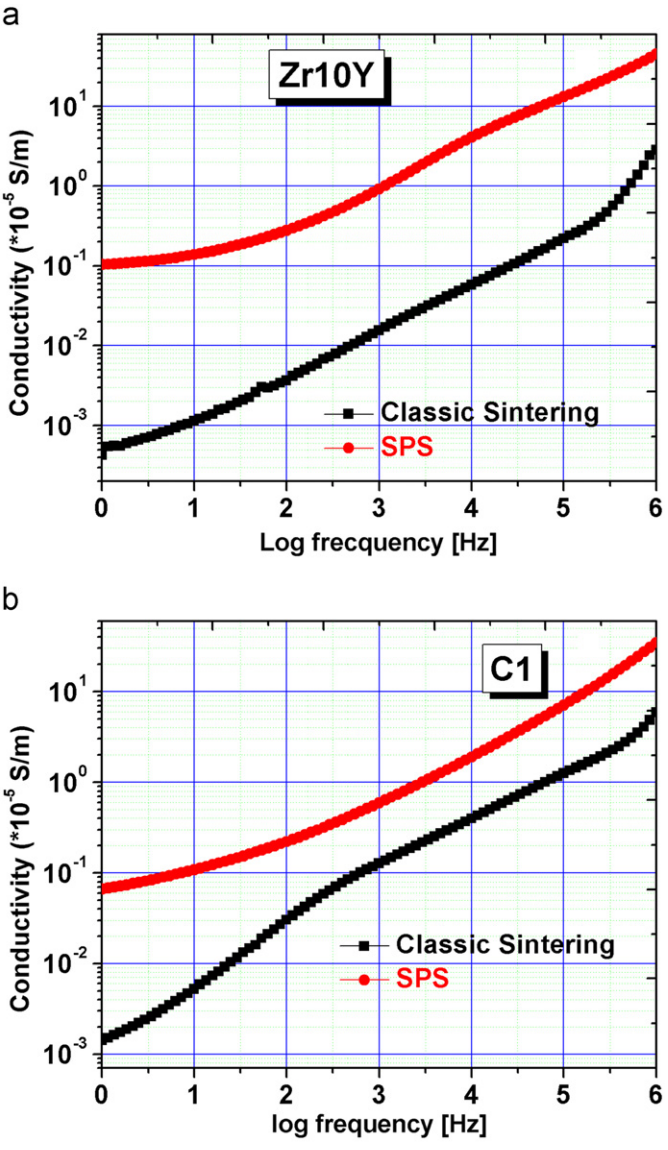

Fig. 9. Frequency dependence of AC conductivity for (a) Zr10Y and (b) C1.

3.3.2. Impedance spectroscopy at high temperature

Fig. 10 presents the imaginary impedance (Z'') as a function of real part of impedance (Z') for each sample at 850 K and 1050 K. At 850 K we can distinguish two distinct semicircles; the first one is the semicircle corresponding to the grain boundary impedance (the semicircle corresponding to the bulk impedance is outside with respect to the frequency scale of the instrumentation at both temperatures) and the second semicircle at low frequency is associated with diffusion of oxygen molecules at the interface between the sample and electrode. At the higher temperature (1050 K), the grain boundary semicircle is off the scale, and only the semicircle attributed to the sample/electrode contact is present.

To determine the total conductivity of the samples, the semicircles in the Nyquist plot were extrapolated to the intersections with the real axis using Zview software.

From the Arrhenius plot (Fig. 11) of total conductivity of the samples, we can see that at 850 °C the sample that

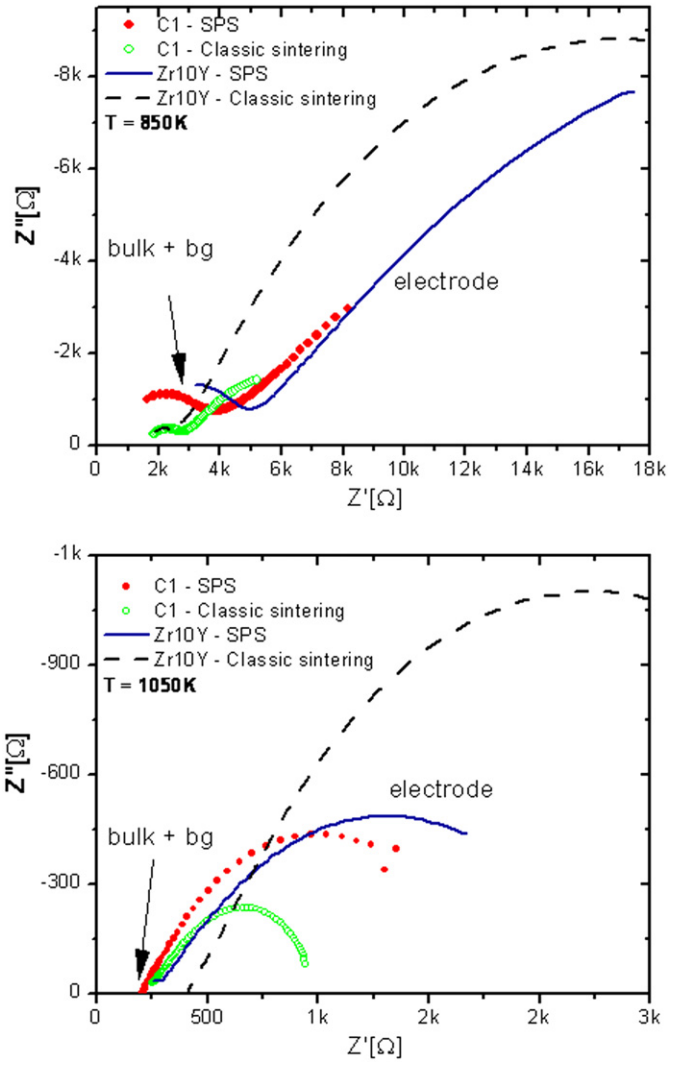

Fig. 10. Impedance experimental spectra presented in the Nyquist plot at 850 K (upper frame) and at 1050 K (lower frame).

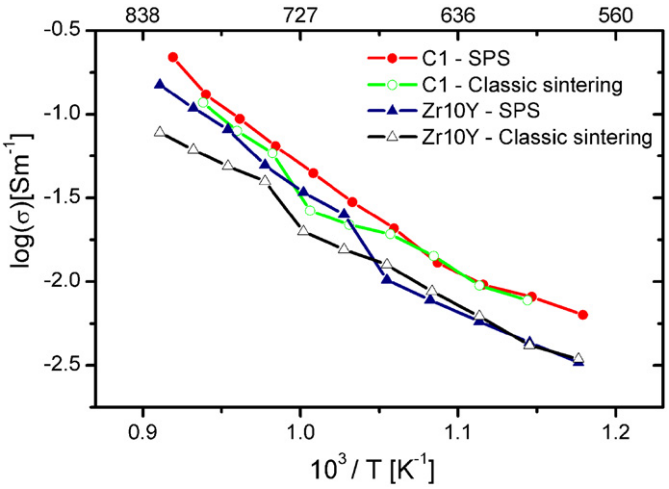

Fig. 11. Temperature dependence of total conductivity of the samples.

Table 1
Total conductivity of samples.

Sample	Total conductivity measured at ~800 °C [S m^{-1}]	Total conductivity at ~1000 °C (calculated by extrapolate the Arrhenius plot) [S m^{-1}])
C1—SPS	2.19×10^{-1}	1.94
C1—1600	1.17×10^{-1}	1.32
Zr10Y—SPS	1.09×10^{-1}	1.07
Zr10Y—1600	6.14×10^{-2}	0.63

presents the highest total conductivity is the nanocomposite sintered through SPS. The values obtained are presented in Table 1. The lowest total conductivity was obtained for the classically sintered yttria stabilized zirconia.

4. Conclusion

Dense cubic zirconia ceramics and zirconia nanocomposites (reinforced with 5% alumina) have been prepared from powders synthetized through sol–gel methods and densified using classical sintering and spark plasma sintering (SPS).

The X-ray diffraction determinations showed the presence of cubic zirconia and alpha alumina.

The scanning electron microscopy and apparent density investigations have proved that highly densified zirconia ceramics and composites samples have been obtained. Using the "spark plasma sintering" method, a nanostructured ceramic has been obtained, with grains varying in size from 53 to 99 nm.

The grain size has a strong influence on the electrical properties. Thus, at room temperature, for the zirconia ceramics sintered through the SPS method, a DC conduction of 10^{-1} S/cm has been obtained, due to the oxygen vacancies. For the composites ceramics, the nanometric grain size of samples induces only one conduction mechanism. At higher temperatures, the nanostructured ceramic samples present a

higher conductivity. Also, the addition of alumina to zirconia improves the total conductivity for both sintering methods, the higher conductivity being obtained for the nanostructured composite sintered through SPS.

References

[1] A. Rizea, D. Chirlesan, C. Petot, G. Petot-Ervas, The influence of alumina on the microstructure and grain, boundary conductivity of yttria-doped zirconia, Solid State Ionics 146 (2002) 341–353.

[2] X.J. Chen, K.A. Khor, S.H. Chan, L.G. Yu, Influence of microstructure on the ionic conductivity of yttria-stabilized zirconia electrolyte, Materials Science and Engineering A 335 (2002) 246–252.

[3] M. Lang, T. Franco, G. Schiller, N. Wanger, Electrochemical characterization of vacuum plasma sprayed thin-film solid oxide fuel cells (SOFC) for reduced operating temperatures, Journal of Applied Electrochemistry 32 (2002) 871–874.

[4] C.J. Li, C.X. Li, X.J. Ning, Performance of YSZ electrolyte layer deposited by atmospheric plasma spraying for cermet-supported tubular SOFC, Vacuum 73 (2004) 699–703.

[5] E. Iguchi, S. Nakamaura, F. Munakata, M. Kurumada, Y. Fujie, Ionic conduction due to oxygen diffusion in $La_{0.8}Sr_{0.2}GaO_{3-\delta}$ electrolyte, Journal of Applied Physics 93 (2003) 3662–3664.

[6] E. Iguchi, S. Mochizuki, Electric conduction and dielectric relaxation processes in solid oxide fuel cell electrolyte $La_{0.5}Sr_{0.5}Ga_{0.6}Ti_{0.4}O_{3-\delta}$, Journal of Applied Physics 96 (2004) 3889–3895.

[7] M.J. Verkerk, A.J.A. Winnubst, A.J. Burggraaf, Effect of impurities on sintering and conductivity of yttria-stabilised zirconia, Journal of Materials Science 17 (1982) 3113–3122.

[8] A.J. Feighery, J.T.S. Irvine, Effect of alumina additions on electrical properties of 8 mol% yttria-stabilised zirconia, Solid State Ionics 121 (1999) 209–216.

[9] E.P. Butler, N. Bonanos, The characterization of ZrO_2 engineering ceramics by AC impedance spectroscopy, Materials Science Engineering 71 (1985) 49–56.

[10] D. Lybye, Y.L. Liu, A study of complex effects of alumina addition on conductivity of stabilised zirconia, Journal of the European Ceramic Society 26 (2006) 599–604.

[11] B.S. Vasile, C. Ghitulica, N. Popescu-Pogrion, S. Constantinescu, I. Mercioniu, R. Stan, E. Andronescu, Structural investigations on yttria-doped zirconia nanopowders obtained by sol–gel method, Journal of Optoelectronics and Advanced Materials 9 (2007) 3774–3780.

[12] G. Bernard-Granger, C. Guizard, Spark plasma sintering of a commercially available granulated zirconia powder: I. Sintering path and hypotheses about the mechanism(s) controlling densification, Acta Materialia 55 (2007) 3493–3504.

[13] G. Bernard-Granger, N. Monchalin, C. Guizard, Comparisons of grain size–density trajectory during spark plasma sintering and hot-pressing of zirconia, Materials Letters 62 (2008) 4555–4558.

[14] X. Miaoa, Y. Chen, H. Guo, K.A. Khor, Spark plasma sintered hydroxyapatite–yttria stabilized zirconia composites, Ceramics International 30 (2004) 1793–1796.

[15] M. Trunec, K. Maca, Z. Shen, Warm pressing of zirconia nanoparticles by the spark plasma sintering technique, Scripta Materialia 59 (2008) 23–26.

[16] D. Ravinder, P.V.B. Reddy, High-frequency dielectric behaviour of Li–Mg ferrites, Materials Letters 57 (2003) 4344–4350.

[17] C. Leon, M.L. Lucia, J. Santamaria, Correlated ion hopping in single-crystal yttria-stabilized zirconia, Physical Review B 55 (1997) 882–887.

[18] I.M. Hodge, M.D. Ingram, A.R. West, Impedance and modulus spectroscopy of polycrystalline solid electrolytes, Journal of Electroanalytical Chemistry 74 (1976) 125–143.

[19] R. Gerhardt, Impedance and dielectric spectroscopy revisited: distinguishing localized relaxation from long-range conductivity, Journal of Physics and Chemistry of Solids 55 (1994) 1491–1605.